

Small-Signal Stability Analysis of Inverter-Fed Power Systems Using Component Connection Method

Wang, Yanbo; Wang, Xiongfei; Chen, Zhe; Blaabjerg, Frede

Published in:
I E E E Transactions on Smart Grid

DOI (link to publication from Publisher):
[10.1109/TSG.2017.2686841](https://doi.org/10.1109/TSG.2017.2686841)

Publication date:
2018

Document Version
Accepted author manuscript, peer reviewed version

[Link to publication from Aalborg University](#)

Citation for published version (APA):
Wang, Y., Wang, X., Chen, Z., & Blaabjerg, F. (2018). Small-Signal Stability Analysis of Inverter-Fed Power Systems Using Component Connection Method. *I E E E Transactions on Smart Grid*, 9(5), 5301-5310. Article 7885512. <https://doi.org/10.1109/TSG.2017.2686841>

General rights

Copyright and moral rights for the publications made accessible in the public portal are retained by the authors and/or other copyright owners and it is a condition of accessing publications that users recognise and abide by the legal requirements associated with these rights.

- Users may download and print one copy of any publication from the public portal for the purpose of private study or research.
- You may not further distribute the material or use it for any profit-making activity or commercial gain
- You may freely distribute the URL identifying the publication in the public portal -

Take down policy

If you believe that this document breaches copyright please contact us at vbn@aub.aau.dk providing details, and we will remove access to the work immediately and investigate your claim.

Small-Signal Stability Analysis of Inverter-Fed Power Systems Using Component Connection Method

Y. Wang, *Member, IEEE*, X. Wang, *Member, IEEE*, Z. Chen, *Senior Member, IEEE*,
and F. Blaabjerg, *Fellow, IEEE*

Abstract--The small time constants of power electronics devices lead to dynamic couplings with the electromagnetic transients of power networks, and thus complicate the modeling and stability analysis of power-electronics-based power systems. This paper presents a computationally-efficient approach to assess the small-signal stability of inverter-fed power systems. The power system is partitioned into individual components, including the power inverters, network impedances, and power loads. The state-space model of individual inverter is first built, where the frequency response and eigenvalue analysis collectively characterize the contributions of different controller parameters to the terminal behavior in a wide frequency range. These component models, together with the network equations, are then algebraically assembled based on the interconnection relations at their terminals. As a consequence, the state matrix of the whole system, which is essential to the system stability analysis, can be reformulated in a computationally-efficient way. The experimental results are finally given to validate the effectiveness of the modeling method and system stability analysis.

Index Terms-- Stability, Small-Signal Model, Time Delay, Inverter-Fed Power System, Component Connection Method

NOMENCLATURE

ω_i -- rotating angle frequency of i th inverter;
 δ_i -- phase angle of output voltage of i th inverter;
 ω_c -- cut off frequency of one-order low-pass filter;
 L_{linei} and R_{linei} -- inductance and resistance of i th line;
 L_{loadi} and R_{loadi} -- inductance and resistance of i th load;
 L_{fi} -- inverter-side inductance of LCL filter;
 L_{ci} -- grid-side inductance of LCL filter;
 C_{fi} -- capacitor of LCL filter;
 V_{busi} -- i th bus voltage;
 $i_{LineDQi}$ -- current of i th line on common frame (D-Q);
 $i_{LoadDQi}$ -- current of i th load on common frame (D-Q);
 v_{oi} -- output voltage of i th DG unit;
 i_{oi} -- output current of i th DG unit;
 v_{odqi} -- voltage command of i th DG unit on individual frame (d-q);
 v_{odqi} -- capacitor voltage of i th DG unit on individual frame (d-q);

i_{odqi} -- output current of i th DG unit on individual frame (d-q);
 v_{invdq}^* -- reference voltage of inverter;
 v_{invdq} -- output voltage of inverter;
 i_{dq}^* -- current command of current controller of i th DG unit;
 i_{dq} -- inverter-side inductance current of i th DG unit;
 p_i , q_i -- instantaneous active and reactive power of i th inverter;
 P_i , Q_i -- average active and reactive power of i th inverter;
 m_{pi} , n_{qi} -- droop coefficient of i th DG unit.

I. INTRODUCTION

The growing penetration of the power electronics-interfaced renewable energy sources lead to the emergence of power-electronic-based power systems into electrical grids, such as wind farms [1], photovoltaic power plants [2], and micro-grids [3]. Those systems are featured with the high efficiency and flexibility in electric power generation and distribution, but are also more susceptible to the network disturbances in a wide frequency range [4]. In inverter-fed power systems, a number of oscillation phenomena have been reported, which includes the low-frequency oscillations caused by the droop-enabled power control [5], and grid synchronization control [6]. In addition, the harmonic-frequency oscillations from hundreds of hertz to several kilohertz maybe happen, which is caused by the interaction of the inner control loops as well as the inductive or capacitive behavior of inverters [7]. It is undoubted that these oscillation phenomena will weaken the power quality and cause the instability of power system.

The state-space approach, which was widely used for the power system stability analysis [8], has been applied to address the instability of the inverter-fed power systems. However, most of the research works concentrated on the low-frequency oscillations associated with the power control loops, e.g. the droop-based power control [5], and the constant power control of active loads [9]. The interaction of the inner current and voltage control loops were commonly neglected [5]. A full-order state-space model including the dynamics of the inner current and voltage loops was developed in [4], where only the low-frequency oscillation modes were identified, and the effect of the digital control delay on the harmonic-frequency modes were overlooked. On the other hand, the incorporation of the delay effect and inner control loops significantly increases the order of the system state matrix. The order-reduced model based on the specific oscillation modes is then needed for the system with a large number of inverters [9].

The work was supported in part by the Danish Council for Strategic Research under the project "Development of a Secure, Economic and Environmentally-friendly Modern Power System" (DSF 09-067255) and European Research Council (ERC) under the European Union's Seventh Framework Program (FP7/2007-2013)/ERC Grant Agreement no. [321149-Harmony].

Y. Wang, X. Wang, Z. Chen and F. Blaabjerg are with the Department of Energy Technology, Aalborg University, Aalborg 9220, Denmark. (ywa@et.aau.dk; xwa@et.aau.dk; fbl@et.aau.dk; zch@et.aau.dk)

The impedance-based method is another stability analysis tool, which predicts the dynamic interactions of inverters based on the ratio of the inverter output impedance to the equivalent grid impedance seen by each inverter [9], [10]. Differing from the state-space approach, the impedance-based analysis is a localized method, which assesses the system stability at the point of connection of each inverter [11]. However, the impedance model only characterizes the input-output relationship instead of the system internal states. It thus fails to perform the sensitivity analysis for identifying the participation of each state into the different oscillation modes.

To overcome the aforementioned drawbacks of the state-space modeling and the impedance-based analysis, this paper presents a system stability analysis based on the Component Connection Method (CCM). The CCM is basically a reformulation of the conventional state-space model according to terminal characteristic. It is a computationally-efficient method to implement system modeling [12]-[13]. In this approach, the power system is first partitioned into individual components which can be represented by diagonal matrices. These component models are then assembled together according to their interconnection relationships at the terminals, which are characterized by a linear algebra matrix. A sparse state matrix can thus be obtained for the composite system model. Hence, compared to the impedance-based method, the CCM keeps the advantage of the component-based modeling procedure, which is scalable for the system with a large number of inverters. It also inherits the participation analysis feature of the state-space approach.

The CCM-based stability analysis was earlier introduced for the large transmission grid with the Thyristor-based Static Var Compensator and High Voltage Direct Current systems [13]-[14]. The main contributions of this work are: (1) A computationally-efficient approach to the small-signal stability assessment of the inverter-fed power system. (2) CCM-based small signal model of voltage-source inverters with multiple control loops, where the frequency response and eigenvalue analysis explain the contributions of different control parameters on terminal characteristic in a wide frequency range. (3) Both low- and high-frequency oscillation modes and the associated controller parameters are identified.

The rest of this paper is organized as follows. In Section II, the principle of CCM is described first. Then, the CCM-based modeling procedure is formulated in detail in Section III. This is followed by the system stability analysis in Section IV, where both the low- and high-frequency oscillation modes are identified. Subsequently, the experimental results are presented in Section V to confirm the effectiveness of the theoretical analysis. Finally, the conclusions are drawn in Section VI.

II. THE BASIC PRINCIPLE OF CCM

This section describes first the basic principle of Component-Connection Method (CCM). As shown in Fig. 1(a), a general circuit diagram of an inverter-fed power system is given to illustrate the application of the CCM. In this work, the small-signal model of each inverter is independently built to characterize the terminal dynamic behavior of inverters, where the output currents of inverters and the voltages at the points of connection are interfacing variables to the network,

and the modeling method can be used for the inverters with different control strategies, either voltage-mode or current-mode control. To address the oscillations in a wide frequency range, the multiple control loops including power control, voltage control, and current control are modeled in this work.

A. Component Connection Method (CCM)

In the procedure, each component is independently modeled. According to the principle of the CCM, the dynamic of the i -th component can be represented by the nonlinear differential equations given in [15], which are given below

$$\dot{x}_i = f_i(x_i, u_i) \quad (1)$$

$$y_i = g_i(x_i, u_i) \quad (2)$$

where x_i , y_i , u_i denote the vectors of states, input, and output variables of the i -th component. The linearized state-space model of the i -th component can be derived as (3) and (4).

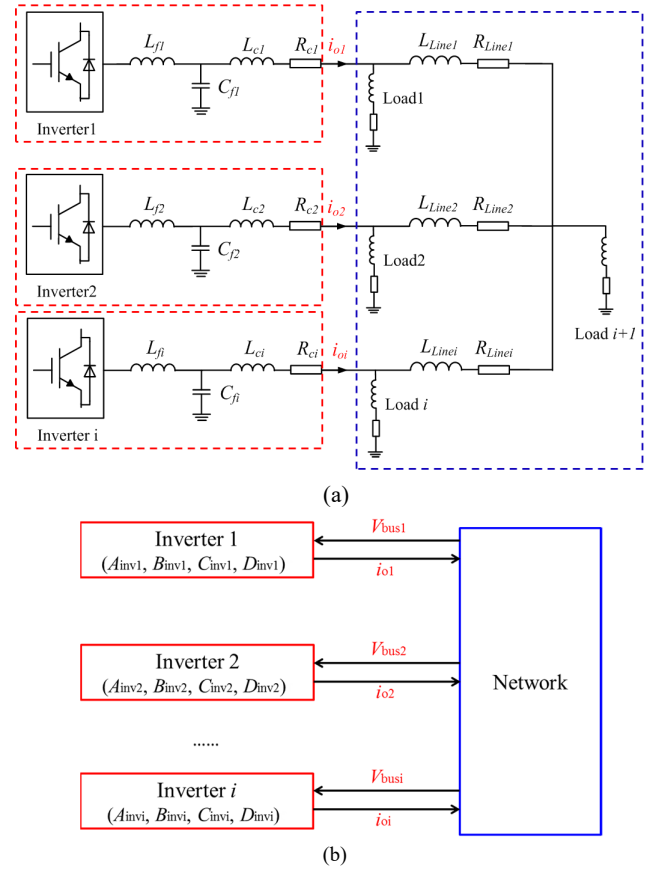


Fig. 1. The diagram of inverter-fed power system applied in CCM. (a) System description. (b) The implementation of system modeling with CCM.

$$\dot{\Delta x}_i = A_i \Delta x_i + B_i \Delta u_i \quad (3)$$

$$\Delta y_i = C_i \Delta x_i + D_i \Delta u_i \quad (4)$$

The sign ' Δ ' in (3) and (4) is removed in the following equations. Then, all the linearized models are assembled together to form a composite system model by diagonal matrices as

$$\dot{x} = Ax + Bu \quad (5)$$

$$y = Cx + Du \quad (6)$$

where A, B, C, D are the diagonal matrices of the composite system, i.e. $A = \text{diag}(A_1, \dots, A_i, \dots, A_n)$, $B = \text{diag}(B_1, \dots, B_i, \dots, B_n)$, $C = \text{diag}(C_1, \dots, C_i, \dots, C_n)$, $D = \text{diag}(D_1, \dots, D_i, \dots, D_n)$, since the components are simply cascaded in diagonal, $x = [x_1, \dots, x_i, \dots, x_n]^T$, $u = [u_1, \dots, u_i, \dots, u_n]^T$, $y = [y_1, \dots, y_i, \dots, y_n]^T$.

are the cascaded vectors of the states, input, and output variables of the components.

As shown in Fig. 1(b), the interconnection relationship among the components can be represented by the algebra equations given as (7) and (8).

$$u = L_1 y + L_2 a \quad (7)$$

$$b = L_3 y + L_4 a \quad (8)$$

where u and y are input and output vectors of the components, a and b are the input and output vectors of the system. L_1, L_2, L_3, L_4 are the component interconnection matrices. The desired state equation and output equation can be obtained by combining (5)-(6) and (7)-(8) as (9) and (10).

$$\dot{x} = Fx + Ga \quad (9)$$

$$b = Hx + Ja \quad (10)$$

where $F = A + BL_1(I - DL_1)^{-1}C$, $G = BL_1(I - DL_1)^{-1}DL_2 + BL_2$, $H = L_3(I - DL_1)^{-1}C$, $J = L_3(I - DL_1)^{-1}DL_2 + L_4$. The system

stability can thus be predicted based on the eigenvalues of the state matrix F . Hence, instead of directly linearizing the nonlinear state-space model of the whole system, the CCM allows independently modeling the input-output relationships of the components and their interconnected network, and assemble them together by means of a simple linear algebraic matrix. In this way, the formulation procedure of the system state matrix can be significantly simplified. Fig. 1(b) depicts the application of the CCM in the studied power system, where the overall system is partitioned into DG inverters, power network and loads.

III. STEP-BY-STEP IMPLEMENTATION OF CCM-BASED MODELING

This section presents the step-by-step implementation of the CCM for modeling the DG inverters and the exemplified system in Fig. 1(a).

A. Component modeling of Inverter

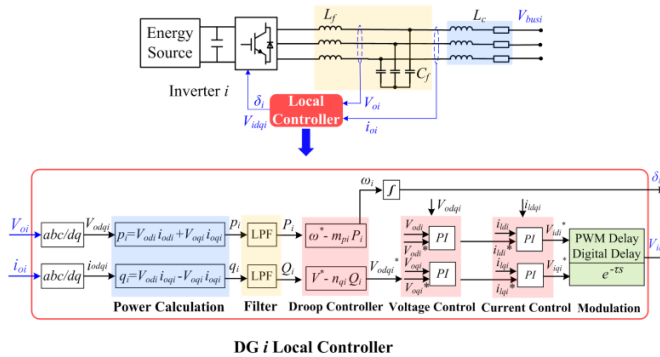


Fig. 2. The diagram of DG inverter with local controller.

Fig. 2 shows the block diagram of the DG inverter with local controller, which is composed of an LCL-filter, the

droop-based power controller, the voltage controller, the current controller and the Pulse Width Modulation (PWM).

The droop-based power controller achieves the power distribution among the paralleled inverters. The averaged active and reactive powers obtained from instantaneous power calculation block are viewed as the reference inputs of the droop controller. The voltage controller and current controller are adopted to perform voltage regulation of inverters. Small signal models of the droop controller, the voltage and current controllers have been well established in [3]-[4]. However, the effect of the time delay involved into the digital control implementation is often overlooked, which has recently been found to have an important impact on the high frequency oscillations [13].

To reveal the effect of time delay, the time delay plant is modeled as (11), which includes one sampling period of digital computational delay (T_s) and the zero-order hold effect of (PWM) ($0.5T_s$).

$$V_i = e^{-\tau s} V_i^* \quad (11)$$

where V_i^* and V_i are the demanded and output voltage of the inverter, respectively. $\tau = 1.5T_s$ is the delay time. In this work, the third-order Pade approximation is used to approximate (11) for the better accuracy, which is given by

$$\frac{120 + 60(\tau s) + 12(\tau s)^2 + (\tau s)^3}{120 + 60(\tau s) + 12(\tau s)^2 + (\tau s)^3} \quad (12)$$

The small signal model of the time delay can be rewritten in a state-space form by (12).

$$\dot{x}_{del} = A_{del} x_{del} + B_{del} V_i^* \quad (13)$$

$$V_i = C_{del} x_{del} + D_{del} V_i^* \quad (14)$$

where $x_{del} = [x_{dq1}, x_{dq2}, x_{dq3}]^T$ are state variables of delay plant (13), $A_{del}, B_{del}, C_{del}, D_{del}$ are the parameter matrices of the delay plant.

$$A_{del} = \begin{bmatrix} A_d & B_d \\ 0 & A_q \end{bmatrix}, \quad B_{del} = \begin{bmatrix} B_d \\ 0 \end{bmatrix}, \quad C_{del} = \begin{bmatrix} C_d & 0 \\ 0 & C_q \end{bmatrix}, \quad D_{del} = \begin{bmatrix} D_d & 0 \\ 0 & D_q \end{bmatrix}, \quad A_d = A_q = \begin{bmatrix} 0 & 1 \\ -120/\tau^3 & -60/\tau^2 - 12/\tau \end{bmatrix}$$

$$B_d = B_q = \begin{bmatrix} 0 & 0 & 1 \end{bmatrix}^T, \quad C_d = C_q = \begin{bmatrix} 240/\tau^3 & 0 & 24/\tau \end{bmatrix}, \quad D_d = D_q = \begin{bmatrix} -1 \end{bmatrix}, \quad V_i^* = [V_{dq}^*]^T, \quad V_i = [V_{dq}]^T$$

The power angle relationship contributes to power distribution among different DG units. The local frame of DG1 ($dq1$) is selected as common frame (DQ), and the dynamics of other DG inverters and power network are transferred into DQ frame. The angle dynamic of the i -th DG can be represented as.

$$\dot{\delta}_i = \omega_i - \omega_{com} \quad (15)$$

And the state-space model of power angle can be given as.

$$\dot{x}_c = A_c x_c + B_c u_c \quad (16)$$

$$y_c = C_c x_c + D_c u_c \quad (17)$$

where $x_c = [\delta_i]$ is the state variable, $u_c = [\omega_i, \omega_{com}]^T$, $y_c = [\delta_i]$, $A_c = 0$, $B_c = \begin{bmatrix} 1 & -1 \end{bmatrix}$, $C_c = 1$, $D_c = \begin{bmatrix} 0 & 0 \end{bmatrix}$.

The mathematical equation of droop controllers can be seen in Fig. 2. The small signal model of the droop controller can be obtained by combining and linearizing power calculation

block, low pass filter block and droop controller, which is given by (18) and (19).

$$\dot{x}_1 = A_1 x_1 + B_1 u_1 \quad (18)$$

$$y_1 = C_1 x_1 + D_1 u_1 \quad (19)$$

where $x_1 = [P_i, Q_i]^T$ is the vector of two state variables, $u_1 = [V_{odi}^*, V_{oqi}^*, i_{odi}^*, i_{oqi}^*]^T$ is the vector of input variables, $y_1 = [V_{odi}^*, V_{oqi}^*, \omega_i]^T$ is the vector of output variables, and A_1, B_1, C_1, D_1 are parameter matrices of the power controller. $A_1 = \begin{bmatrix} 0 & -\omega_i \\ \omega_i & 0 \end{bmatrix}$, $B_1 = \begin{bmatrix} \omega_i i_{odi0} & -\omega_i i_{oqi0} & -\omega_i V_{odi0} & \omega_i V_{oqi0} \end{bmatrix}$, $C_1 = \begin{bmatrix} 0 & 0 \\ -m_{pi} & 0 \end{bmatrix}$, $D_1 = [O_{2 \times 4}]$. $i_{odi0}, i_{oqi0}, V_{odi0}, V_{oqi0}$ are the initial

states of the output current and voltage of the i -th DG inverter.

As shown in Fig. 2, the control system of individual inverter is composed of droop-based power controller, current controller, voltage controller and Pulse Width Modulation (PWM). The voltage and current controller are performed by classical PI controller, which can be seen in [3]–[6]. Together with the small signal models of power angle relationship, power controller, voltage and current controller, LCL filter, and time delay, the component model of DG inverter is formulated as (20) and (21).

$$\dot{x}_{invi} = A_{invi} x_{invi} + B_{invi} u_i \quad (20)$$

$$y_i = C_{invi} x_{invi} \quad (21)$$

where $x_{invi} = [\delta_i, P_i, Q_i, \varphi_{dqi}, \gamma_{dqi}, i_{ldqi}, v_{odqi}, i_{odqi}, x_{del}]^T$ is the vector of 19 state variables of inverter, including the states of power angle (δ_i), droop controller (P_i, Q_i), voltage controller (φ_{dqi}), current controller (γ_{dqi}), LCL filter ($i_{ldqi}, v_{odqi}, i_{odqi}$), and delay plant (x_{del}). Bus voltages (V_{busi}) and command current (i_{odqi}^*) are defined as input vector of inverter, $u_i = [i_{odqi}^*, V_{busi}]^T$. And output current of inverter (i_{odqi}) is selected as the component output (y_i) to connect power network. The terminal characteristic of inverter may be revealed by the closed-loop output admittance and closed-loop gain [10], which can be derived by the ratio of output current to inverter input as (22).

$$\frac{y_i(s)}{u_i(s)} = \frac{C_{invi}(s) \cdot B_{invi}(s)}{A_{invi}(s) + B_{invi}(s) \cdot C_{invi}(s)} \quad (22)$$

Note that if the bus voltage (V_{busi}) is selected as inverter input, the ratio of output to input is closed-loop output admittance. Alternatively, if the command current (i_{odqi}^*) is selected as inverter input, the ratio of output to input is inverter closed-loop gain.

B. Terminal dynamic behavior of Inverter

The frequency response shows the impact of controller parameters on terminal dynamic behavior, and the eigenvalue trace commonly shows the different oscillation modes and damping characteristic. In this work, the merits of two domains are combined to provide comprehensive insights in a wide frequency range. The terminal characteristic of the inverter can be represented by output admittance in impedance model (22), which is able to directly reveal the contributions of different controller parameters in a wide frequency range. In this section, the impact of droop controller, voltage

controller, current controller and time delay on terminal dynamic behavior is investigated.

(1) The impact of droop controller on terminal behavior

To reveal the impact of droop controller on terminal dynamic behavior, the frequency response and eigenvalue trace of inverter is given in Fig. 3, which shows the terminal dynamic characteristic of individual inverter as the increase of reactive power-voltage droop coefficient ($1e-3$ to $5e-3$, step: $1e-3$). It can be seen that the terminal characteristic of inverter in low frequency range (1Hz-10Hz) is significantly affected by reactive power droop coefficient, while the dynamic characteristic in high-frequency range is slightly affected.

(2) The impact of voltage and current controller on terminal behavior

To investigate the impact of voltage and current controller on terminal dynamic behavior, the frequency response and eigenvalue trace of inverter are shown in Fig. 4 and Fig. 5, which shows the terminal characteristic of inverter as the increase of proportional gain of voltage controller. It can be observed that the proportional gain of voltage controller and current controller have dramatic effects on high-frequency performance of inverter (500 Hz-1000 Hz), and the eigenvalue trace of individual inverter also indicates the same effect in high-frequency range.

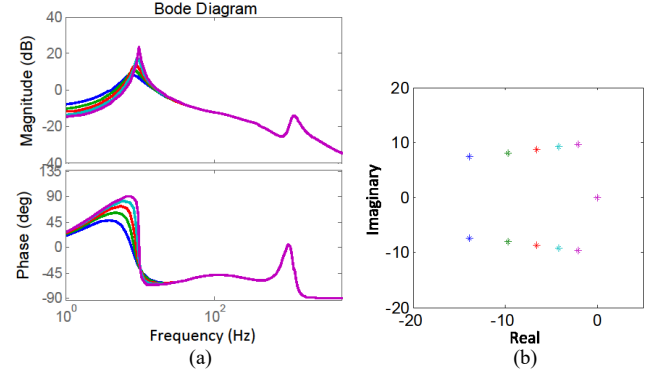


Fig. 3. Terminal characteristic of inverter as the increase of droop coefficient ($1e-3$ to $5e-3$, step: $1e-3$) without considering time delay. (a). Frequency response of inverter terminal characteristic. (b). Eigenvalue trace of individual inverter.

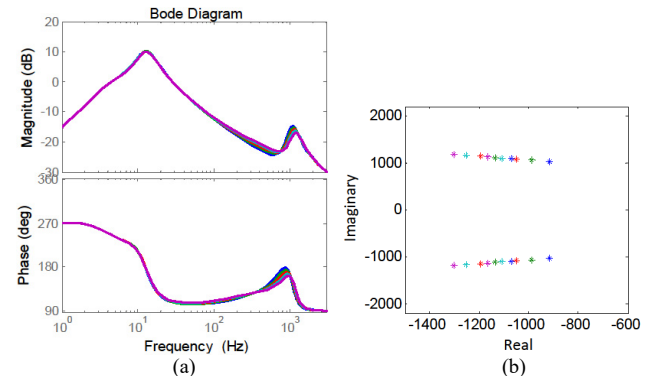


Fig. 4. Terminal characteristic of inverter as the increase of proportional gain of voltage controller (0.01 to 0.05, step: 0.01) without considering time delay. (a). Frequency response of inverter terminal dynamic behavior. (b). Eigenvalue trace of individual inverter.

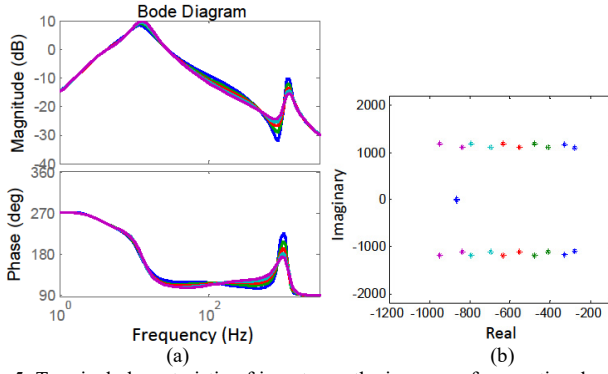


Fig. 5. Terminal characteristic of inverter as the increase of proportional gain of current controller (2 to 6, step: 1) without considering time delay. (a). Frequency response of inverter terminal dynamic behavior. (b). Eigenvalue trace of individual inverter.

(3) The impact of time delay on terminal behavior

Once time delay is considered, the terminal behavior will be dramatically affected. Fig. 6 shows the frequency response of individual inverter with the increase of sampling time.

Fig. 6(a) shows the frequency response characteristic of inverter output admittance as the increase of sampling time. It can be seen that the time delay has an essential effect on high-frequency performance of inverter output admittance.

The frequency response obtained from Fig. 3-6 shows that the controller parameters in multiple control loops have different contributions on inverter terminal behavior in different frequency range.

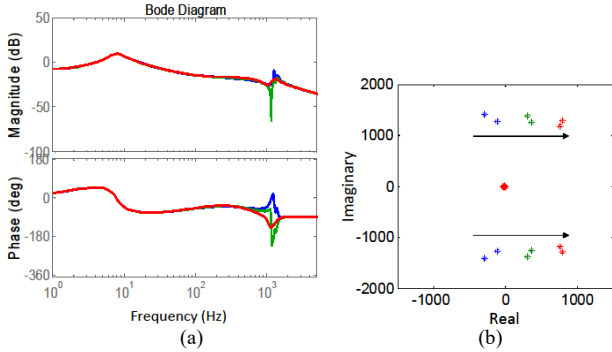


Fig. 6. Terminal characteristic of inverter as the increase of sampling time ($T_s=1/10000, 1/8000, 1/6000$). (a). Frequency response of inverter terminal behavior. (b). Eigenvalue trace of individual inverter.

C. Component modeling of Power Network and Loads

The power network and loads as shown in Fig. 7 are modeled as individual components. The different inverter components are connected and coupled by power network.

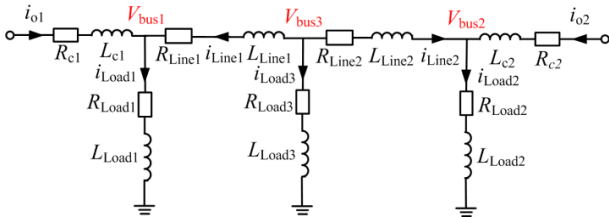


Fig. 7. Component of network and loads

The state equations of the i -th line current and load current on the DQ frame could be represented as (23) and (24).

$$\begin{aligned} \dot{i}_{LineDi} &= \frac{-R_{Linei}}{L_{Linei}} i_{LineDi} - \omega_{com} i_{LineQi} - \frac{1}{L_{Linei}} V_{busDi} + \frac{1}{L_{Linei}} V_{busD3} \\ \dot{i}_{LineQi} &= \frac{-R_{Linei}}{L_{Linei}} i_{LineQi} + \omega_{com} i_{LineDi} - \frac{1}{L_{Linei}} V_{busQi} + \frac{1}{L_{Linei}} V_{busQ3} \end{aligned} \quad (i=1,2) \quad (23)$$

$$\begin{aligned} \dot{i}_{LoadDi} &= \frac{-R_{Loadi}}{L_{Loadi}} i_{LoadDi} - \omega_{com} i_{LoadQi} + \frac{1}{L_{Loadi}} V_{busDi} \\ \dot{i}_{LoadQi} &= \frac{-R_{Loadi}}{L_{Loadi}} i_{LoadQi} + \omega_{com} i_{LoadDi} + \frac{1}{L_{Loadi}} V_{busQi} \end{aligned} \quad (i=1,2,3) \quad (24)$$

The linearized state equations of lines and loads can be given as (25)-(26) by linearizing (23)-(24).

$$\Delta i_{LineDQi} = A_{Line1i} \Delta \omega_{com} + A_{Line2i} \Delta i_{LineDQi} + A_{Line3i} V_{busDQi} + A_{Line4i} V_{busDQ3}$$

$$\Delta \dot{i}_{LoadDQi} = A_{Load1i} \Delta \omega_{com} + A_{Load2i} \Delta i_{LoadDQi} + A_{Load3i} V_{busDQi} \quad (25)$$

$$A_{Line1i} = \begin{bmatrix} -\frac{R_{Linei}}{L_{Linei}} & -\omega_0 \\ \omega_0 & -\frac{R_{Linei}}{L_{Linei}} \end{bmatrix}, \quad A_{Line2i} = \begin{bmatrix} -\frac{1}{L_{Linei}} & 0 \\ 0 & \frac{1}{L_{Linei}} \end{bmatrix}, \quad A_{Line3i} = \begin{bmatrix} \frac{1}{L_{Linei}} & 0 \\ 0 & \frac{1}{L_{Linei}} \end{bmatrix}, \quad A_{Line4i} = \begin{bmatrix} -\frac{1}{L_{Linei}} & 0 \\ 0 & \frac{1}{L_{Linei}} \end{bmatrix}$$

$$A_{Load1i} = \begin{bmatrix} -\frac{R_{Loadi}}{L_{Loadi}} & -\omega_0 \\ \omega_0 & -\frac{R_{Loadi}}{L_{Loadi}} \end{bmatrix}, \quad A_{Load2i} = \begin{bmatrix} \frac{1}{L_{Loadi}} & 0 \\ 0 & \frac{1}{L_{Loadi}} \end{bmatrix}, \quad A_{Load3i} = \begin{bmatrix} \frac{1}{L_{Loadi}} & 0 \\ 0 & \frac{1}{L_{Loadi}} \end{bmatrix}, \quad A_{Load4i} = \begin{bmatrix} -\frac{1}{L_{Loadi}} & 0 \\ 0 & \frac{1}{L_{Loadi}} \end{bmatrix}$$

In this work, virtual resistors are introduced between node and ground to simplify voltage equations [4]. The influence of the virtual resistor on the system stability will be analyzed later. Then, the node voltages can be represented on the common DQ frame as (27) and (28).

$$V_{busDQi} = r_N (i_{oDQi} + i_{LineDQi} - i_{LoadDQi}) \quad (27)$$

$$V_{busDQ(i+1)} = r_N (-i_{LineDQi} - \dots - i_{LineDQi} - \dots - i_{LoadDQ(i+1)}) \quad (28)$$

D. Algebra Interconnection of Components

The advanced merit of CCM is to combine different components by algebra interconnection, where only input-output relationship is concerned and the state matrix is reformulated in a computationally-efficient way.

The component model of the power network and loads are obtained by combining (27) and (28) as (29).

$$y_{net} = C_{net} x_{net} \quad (29)$$

where $x_{net} = [i_{LineDQ1}, \dots, i_{LineDQi}, i_{LoadDQ1}, \dots, i_{LoadDQi}]^T$ is the vector of state variables of the network and loads, $A_{net} = \text{diag}(A_{Line21}, A_{Line22}, A_{Load21}, A_{Load22}, A_{Load23})$, $u_{net} = [V_{bus1}, \dots, V_{busi}, \omega_{com}]^T$, $y_{net} = [i_{LineDQ1}, \dots, i_{LineDQi}, i_{LoadDQ1}, \dots, i_{LoadDQi}]^T$.

Finally, the composite system model is formulated by combining (20), (21) and (29) as (30).

$$y_T = C_T x_T \quad (30)$$

$A_T = \text{diag}(A_{inv1}, \dots, A_{inv}, A_{net})$, $B_T = \text{diag}(B_{inv1}, \dots, B_{inv}, B_{net})$, $C_T = \text{diag}(C_{inv1}, \dots, C_{inv}, C_{net})$, $x_T = [x_{inv1}, \dots, x_{inv}, x_{net}]^T$ are state variables of network and loads.

The input variable of inverter model (20) can be rewritten by sparse matrix L_i as (31) and the input variable of network component (29) may be rewritten by sparse matrix L_{net} as (32).

$$u_i = L_i y_i \quad (i=1,2,\dots,k) \quad (31)$$

$$u_{net} = L_{net} y_{net} \quad (32)$$

Then, the interconnection relationship between component inputs and outputs can be given by combining (31) and (32) as (33).

$$u_T = L_T y_T \quad (33)$$

where $u_T = [u_1, u_2, \dots, u_k, u_{net}]^T$, $y_T = [y_1, y_2, \dots, y_k, y_{net}]^T$, $L_T = \text{diag}(L_1, L_2, \dots, L_k, L_{net})$

The composite system model can be obtained by according to (30) and (33) as (34).

$$\dot{x} = Fx \quad (34)$$

where $F = A_T + B_T L_T C_T$. In the modeling procedure, each inverter component is connected to power system according to terminal characteristic, so that the system model can be extended easily as the increase of inverters and power loads.

IV. SMALL-SIGNAL STABILITY ASSESSMENT

The eigenvalues of state matrix (F) is able to indicate the stability and damping characteristic. In this work, the eigenvalue trajectory of state matrix is calculated to assess the small-signal stability in a wide frequency range caused by multiple control loops. The test system parameters are listed in Table I.

Table I Test System Parameters

Parameters	Value	Parameters	Value
Rated Voltage	220 V	Frequency	50 Hz
DC Voltage	750V	Switching Frequency	10 kHz
L_{f1}/L_{f2}	1.5 mH/1.5 mH	T_s	100 μ s
C_{f1}/C_{f2}	25 μ F/25 μ F	L_{Load1}/R_{Load1}	155 mH/64 Ω
L_{c1}/L_{c2}	1.8 mH/1.8 mH	L_{Load2}/R_{Load2}	156 mH/64 Ω
L_{Line1}/R_{Line1}	1.8 mH/0.2 Ω	L_{Load3}/R_{Load3}	245 mH/80 Ω
L_{Line2}/R_{Line2}	1.8 mH/0.2 Ω	m_{p1}/m_{p2}	1e-4/1e-4
n_{q1}/n_{q2}	1e-3/1e-3	K_{pv1}/K_{pv2}	(0.04-0.056)
K_{iv1}/K_{iv2}	100/100	K_{pc1}/K_{pc2}	(8-12)

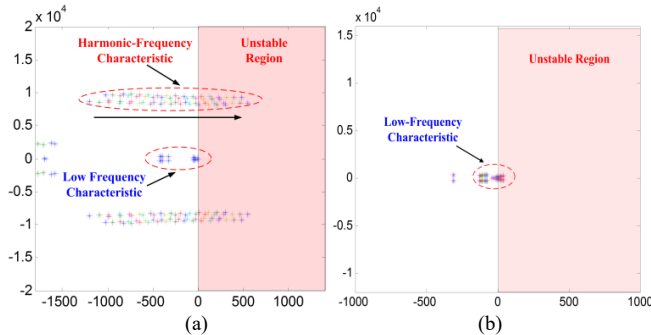


Fig. 8. Eigenvalue trace diagram of the small signal model. (a) The proposed small signal model with considering time delay. (b) Conventional small signal model without considering time delay.

Fig. 8(a) shows that the eigenvalue trace diagram of small signal model considering time delay of digital control system.

It can be seen from Fig. 8(a) that the time delay has a dramatic effect on harmonic-frequency (8000 rad/s) oscillation modes. As the increase of proportional gains of inner controller, the harmonic-frequency modes move towards unstable region. In contrast, the eigenvalue trace diagram without considering time delay is shown in Fig. 8(b), where the harmonic-frequency oscillation characteristic are far away from unstable region, which are not dominant poles and slightly affects system stability. Hence, the high-frequency oscillation modes caused by time delay fail to be observed by previous small signal models.

A. Low-frequency Oscillation Assessment

An inverter-fed power system with 2 inverters is first modelled to perform low-frequency instability assessment. The effect of active power and reactive power droop gains on low-frequency oscillation is investigated in this section. Fig.9(a) shows the low-frequency (20-70 rad/s) eigenvalue trace as the active power droop gain (m_p) of power controllers increases from 0.1e-3 to 3e-3. The oscillation modes will move toward the right-half plane (unstable region) as the increase of active power droop coefficients. It is apparent that the oscillation modes represent the dynamics of active power sharing among inverters. Also, Fig. 9(b) shows the low-frequency oscillation modes move towards the right-half plane (unstable region) as the increase of the reactive power droop coefficients.

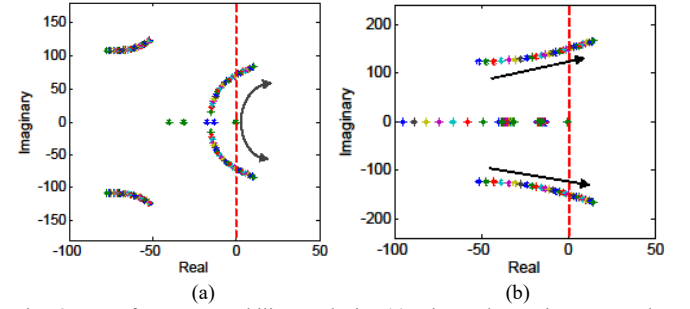


Fig. 9. Low-frequency stability analysis. (a) Eigenvalue trajectory as the increase of active power droop gains of power controller (0.1e-3 < m_p < 3e-3). (b) Eigenvalue trajectory as the increase of reactive power droop gain of power controllers (1e-3 < n_q < 30e-3).

B. High-frequency Instability assessment

Furthermore, the high-frequency (9000 rad/s) stability is assessed for the exemplified power system. Fig. 10(a) shows the eigenvalue traces of the composite model (34) when the proportional gain of voltage controllers increase. It can be seen that two complex-conjugate pairs dominate the high-frequency oscillation modes. These eigenvalues are highly sensitive to the proportional gain of voltage controller, where the modes represent the high-frequency dynamics. The eigenvalue analysis shows that the modes move towards the right-half plane (unstable region) as K_{pv} increases. It can also be seen that the high frequency modes are sensitive to the parameters of the voltage controller.

Fig. 10(b) shows the eigenvalue trace of high frequency modes when the proportional gain of current controller is within the range from 2 to 12, where the high frequency modes move towards the right-half plane as K_{pc} increases. The system would be unstable if K_{pc} is larger than 9.

As demonstrated in Section II, virtual resistors were introduced to define node voltages. In this section, the influence of virtual resistor on the system stability is investigated. Fig. 11 shows the eigenvalue trajectory as the increase of virtual resistor from 600 Ω to 1000 Ω . It can be observed that virtual resistors have an essential effect on the fundamental frequency oscillation modes (50Hz), and slightly

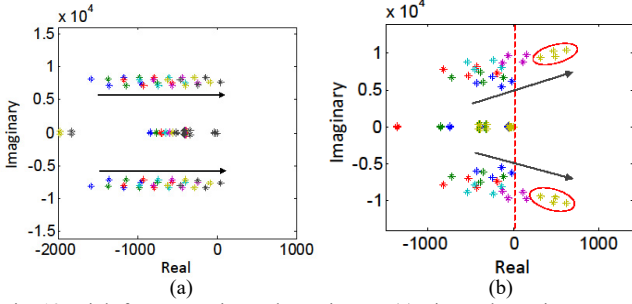


Fig. 10. High-frequency eigenvalue trajectory (a) Eigenvalue trajectory as the increase of proportional gain of voltage controller ($0 < K_{pv} < 0.06$). (b) Eigenvalue trajectory as the increase of proportional gain of current controller ($2 < K_{pc} < 12$).

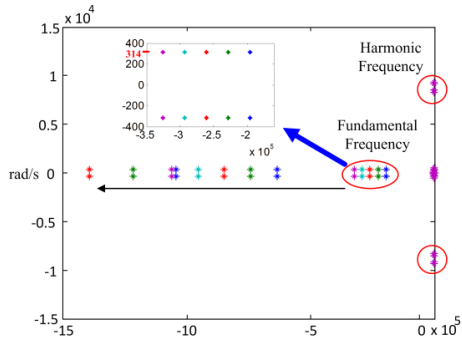
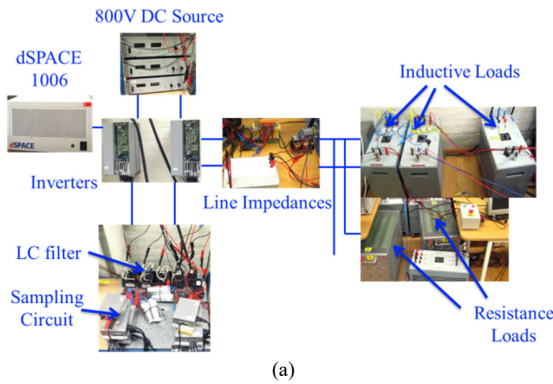


Fig. 11. The eigenvalue trajectory as the increase of virtual resistor (r_n) ($600 \Omega < r_n < 1000 \Omega$).

V. EXPERIMENTAL VERIFICATION

To validate the CCM-based small-signal stability analytical method, the experimental verification is performed. The photograph and configuration of test system is shown in Fig.12, and the system parameters are listed in Table I.



(a)

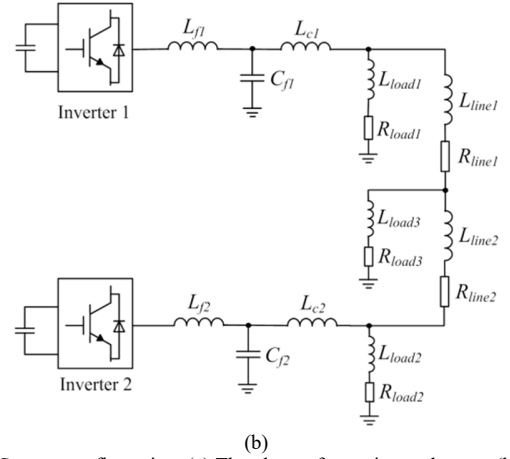


Fig. 12. System configuration. (a) The photo of experimental setup. (b) Circuit configuration.

A. Low-frequency Instability Assessment

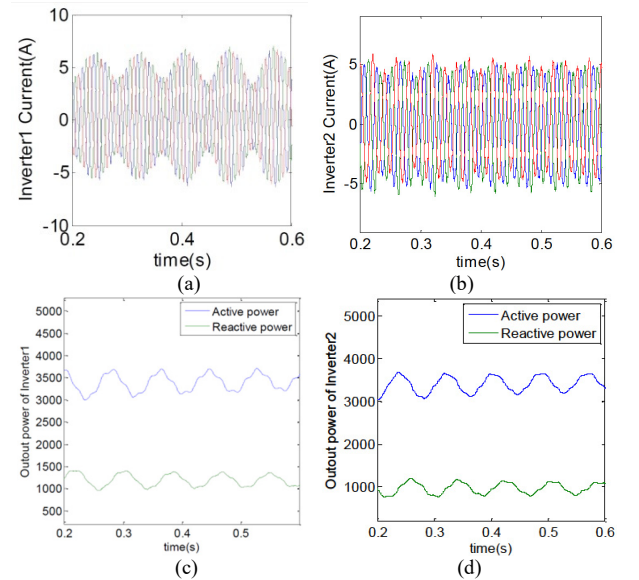


Fig. 13. Experimental results in the low-frequency oscillation case ($m_p = 0.62e-3$, $n_p = 1e-3$). (a) Inverter1 output current. (b) Inverter2 output current. (c) Inverter1 output power. (d) Inverter2 output power.

Fig. 13 shows that the experimental results in low-frequency oscillation case when the active power droop gain (m_p) of the power controllers increase. Fig. 13(a)-(b) shows the output current of inverter1 and inverter2. Also, Fig. 13(c)-(d) shows the output power of inverter1 and inverter2, respectively. Fig.14 shows that the experimental results in the low-frequency oscillation case when the reactive power droop gain (n_q) of the power controller increases, where the output current of inverter1 and inverter2 is shown in Fig. 14(a)-(b). Fig.14(c)-(d) shows the output power of inverter1 and inverter2, respectively.

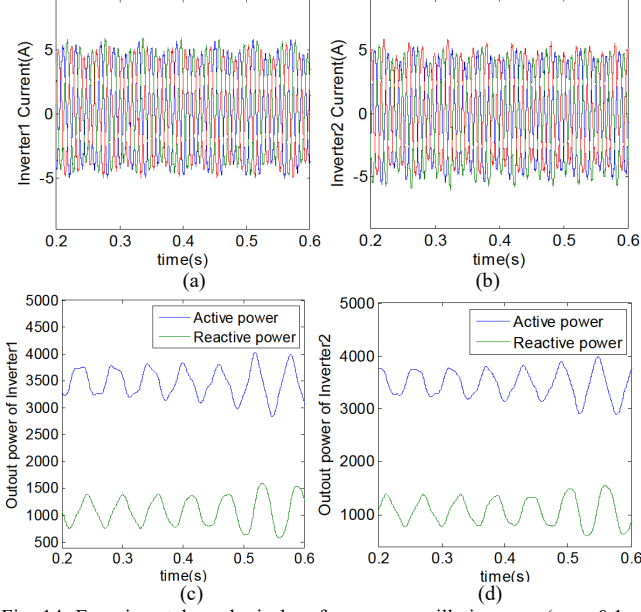


Fig. 14. Experimental results in low-frequency oscillation case ($m_p = 0.1e-3$, $n_p = 18e-3$). (a) Inverter1 output current. (b) Inverter2 output current. (c) Inverter1 output power. (d) Inverter2 output power.

B. High-frequency instability assessment

Fig. 15 shows that the experimental results in the unstable case when the proportional gains (K_{pv}) of the voltage controller vary. The output current of the inverters and network voltages are depicted in Fig. 15(a)-(b) and Fig. 15(c)-(d). It can be seen that the high-frequency oscillation happens, when the proportional gains (K_{pv}) of the voltage controllers are set as 0.056.

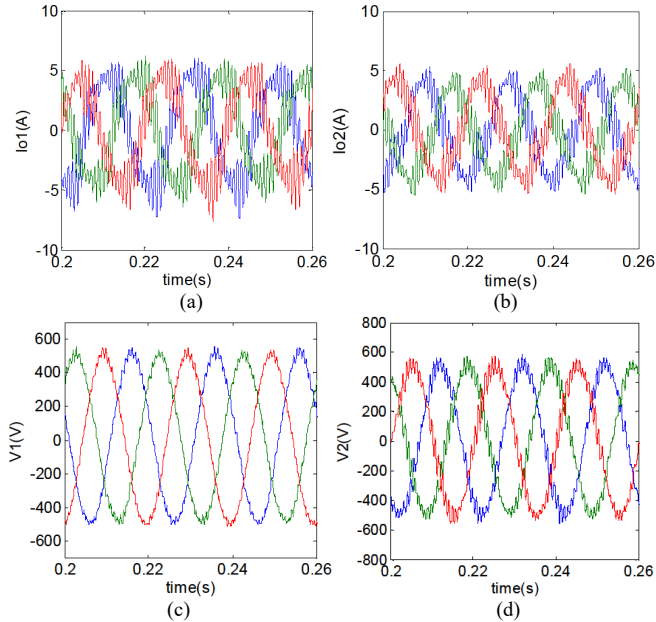


Fig. 15. Experimental results in the unstable case ($K_{pv}=0.053$, $K_{pc}=8$). (a) Inverter1 output current. (b) Inverter2 output current. (c) Bus1 phase-to-phase voltage. (d) Bus2 phase-to-phase voltage.

On the contrary, the output current of the inverters and network voltages are stabilized as shown in Fig. 16(a)-(b) and Fig. 16(c)-(d) after decreasing the proportional gains of the controllers.

Fig. 17 depicts the experimental results in the unstable case, when the proportional gains (K_{pc}) of the current controller are in the unstable region. The output current of inverters and network voltages are depicted in Fig. 17(a)-(b) and Fig. 17(c)-(d), respectively. It can be seen that high-frequency oscillation still happens, when the proportional gains (K_{pc}) of the current controller are set as 11. The results from the eigenvalue analysis agree with the experimental results. The simulation and experimental results, together with analysis results shown in Fig. 10, indicate that the high proportional gains of inner control loops result in the harmonic-frequency oscillations.

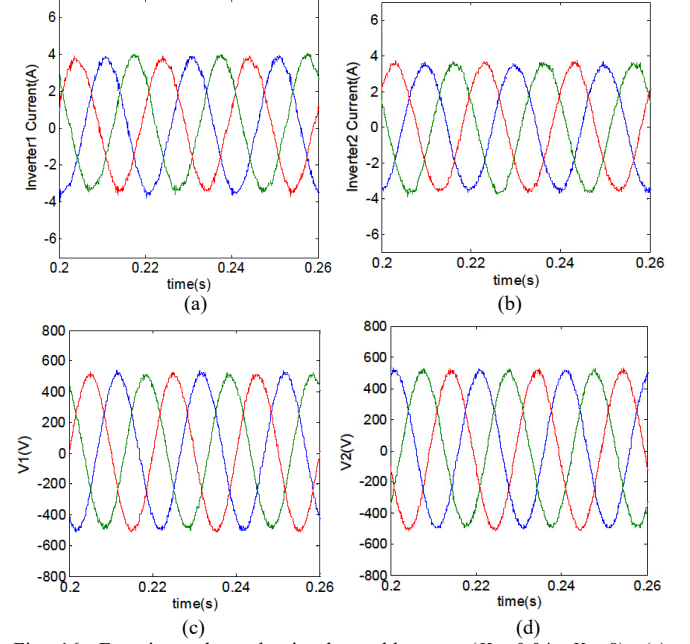


Fig. 16. Experimental results in the stable case ($K_{pv}=0.04$, $K_{pc}=8$). (a) Inverter1 output current. (b) Inverter2 output current. (c) Bus1 phase-to-phase voltage. (d) Bus2 phase-to-phase voltage.

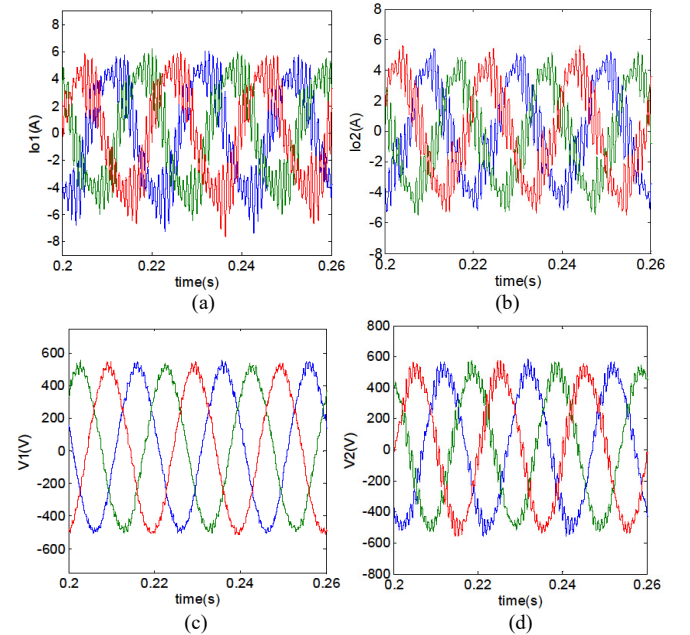


Fig. 17 Experimental results in unstable case ($K_{pv}=0.04$, $K_{pc}=12$). (a) Inverter1 output current. (b) Inverter2 output current. (c) Bus1 phase-to-phase voltage. (d) Bus2 phase-to-phase voltage.

VI. CONCLUSION

This paper addresses a CCM-based modeling and small-signal stability analysis method for inverter-fed power system used in different frequency range. First, the power system is partitioned into different components, and each component is independently modeled. Then, all the component models are assembled to form a composite system model according to terminal interconnection relationship. The terminal characteristic of inverter is investigated by means of frequency response and eigenvalue trace analysis. Finally, an eigenvalue-based approach is proposed to assess low-frequency and high-frequency instability, the influence of controller parameters on small-signal stability is assessed through the eigenvalue trace diagram. The analytical results show that both low-frequency and high-frequency instability may happen in inverter-fed power system, which indicates the parameters of multiple control loops have different contributions on instability phenomena in a wide frequency range. Experimental results are given for validating the proposed stability analytical method.

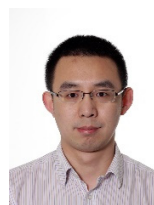
REFERENCES

- [1] F. Blaabjerg, R. Teodorescu, M. Liserre, and A. V. Timbus, "Overview of control and grid synchronization for distributed power generation systems," *IEEE Trans. on Power. Electron.*, vol. 53, no. 5, pp. 1389-1409, Oct. 2006.
- [2] J. L. Agorreta, M. Borrega, J. Lopez, and L. Marroyo, "Modeling and control of N-paralleled grid-connected inverters with LCL filter coupled due to grid impedance in PV plants," *IEEE Trans. on Power. Electron.*, vol. 26, no. 3, pp. 770-785, Mar. 2011.
- [3] Y. Wang, Z. Chen, X. Wang, Y. Tian, Y. Tan, and C. Yang, "An estimator-based distributed voltage-predictive control strategy for AC islanded microgrids," *IEEE Trans. on Power. Electron.*, vol. 30, no. 7, pp. 3934-3951, Jul. 2015.
- [4] N. Pogaku, M. Prodanovic, and T. C. Green, "Modeling, analysis and testing of autonomous operation of an inverter-based microgrid," *IEEE Trans. Power. Electron.*, vol. 22, no. 2, pp. 613-625, Mar. 2007.
- [5] E. A. A. Coelho, P. C. Cortizo, P. F. D. Garcia, "Small-signal stability for parallel-connected inverters in stand-alone AC supply systems," *IEEE Trans. Ind Applications*, vol. 38, no. 2, pp. 533-542, Mar. 2002.
- [6] Z. Xin, X. Wang, P. C. Loh, and F. Blaabjerg, "Grid-current feedback control for LCL-filtered grid converters with enhanced stability," *IEEE Trans. on Power. Electron.*, vol. 32, no. 4, pp. 3216-3228, Apr. 2017.
- [7] X. Wang, F. Blaabjerg, M. Liserre, Z. Chen, J. He, and Y. Li, "An active damper for stabilizing power-electronics-based AC systems," *IEEE Trans. Power. Electron.*, vol. 29, no. 7, pp. 3318-3329, Jul. 2012.
- [8] P. Kundur, *Power system stability and control*. New York: McGraw-Hill, 1994.
- [9] Y. Wang, X. Wang, F. Blaabjerg, and Z. Chen, "Harmonic instability assessment using state-space modeling and participation analysis in inverter-fed power systems," *IEEE Trans. Ind Electron.*, vol. 64, no. 1, pp. 806-816, Jan. 2017.
- [10] J. Sun, "Impedance-based stability criterion for grid-connected inverters," *IEEE Trans. Power Electron.*, vol. 26, no. 11, pp. 3075-3078, Nov. 2011.
- [11] R. Middlebrook, "Input filter considerations in design and application of switching regulators," in *Proc. IEEE Ind. Appl. Soc. Annu. Meet.*, pp. 366-382, 1976.
- [12] G. Gaba, S. Lefebvre, and D. Mukhedkar, "Comparative analysis and study of the dynamic stability of AC/DC systems," *IEEE Trans. Power Syst.*, vol. 3, no. 3, pp. 978-985, Aug. 1988.
- [13] S. Arabi, G. J. Rogers, D. Y. Wong, P. Kundur, and M. G. Lauby, "Small signal stability program analysis of SVC and HVDC in AC power systems," *IEEE Trans. Power Syst.*, vol. 6, no. 3, pp. 1147-1153, Aug. 1991.
- [14] M. A. Choudhry, A. S. Emarah, K. A. Ellithy, and G. D. Galanos, "Stability analysis of a modulated AC/DC system using the eigenvalue sensitivity approach," *IEEE Trans. Power Syst.*, vol. PWRS-1, no. 2, pp. 128-136, May. 1986.
- [15] H. K. Khalil, "Nonlinear System," 3rd ed. Englewood Cliffs, NJ: Prentice-Hall, 2002.
- [16] G. Hou, and V. Vittal, "Trajectory sensitivity based preventive control of voltage instability considering load uncertainties," *IEEE Trans. Power Syst.*, vol. 27, no. 4, pp. 2280-2288, Nov. 2012.
- [17] J. Wang, J. D. Yan, L. Jiang, and J. Zou, "Delay-dependent stability of single-loop controlled grid-connected inverters with LCL filters," *IEEE Trans. Power Electron.*, vol. 30, no. 12, pp. 6520-6523, Feb. 2015.
- [18] S. Buso, and P. Mattavelli, *Digital Control in Power Electronics*. CA, USA: Morgan & Claypool Publishers, 2006.
- [19] P. Cortes, J. Rodriguez, C. Silva, and A. Flores, "Delay compensation in model predictive current control of a three-phase inverter," *IEEE Trans. Ind Electron.*, vol. 59, no. 2, pp. 1323-1325, Feb. 2012.



Yanbo Wang (S'15-M'17) received the M.S. degrees in electrical engineering in the Electrical Engineering School, Southwest Jiaotong University, Chengdu, China, in 2011. He is currently working toward the Ph.D degree in the department of Energy Technology, Aalborg University, Denmark.

His research interests include harmonic analysis and mitigation in power electronic-fed power system, distributed power generation system, microgrid, power system state estimation and stability analysis.



Xiongfei Wang (S'10-M'13) received the B.S. degree from Yanshan University, Qinhuangdao, China, in 2006, the M.S. degree from Harbin Institute of Technology, Harbin, China, in 2008, both in electrical engineering, and the Ph.D. degree in energy technology from Aalborg University, Aalborg, Denmark, in 2013. Since 2009, he has been with the Aalborg University, Aalborg, Denmark, where he is currently an Associate Professor in the Department of Energy Technology. His research

interests include modeling of power electronic converters, harmonics analysis and control, passive and active filters, stability of power-electronic-based power systems.

Dr. Wang serves as an Associate Editor for the IEEE TRANSACTIONS ON POWER ELECTRONICS, the IEEE TRANSACTIONS ON INDUSTRY APPLICATIONS, and the IEEE JOURNAL OF EMERGING AND SELECTED TOPICS IN POWER ELECTRONICS. He received the second prize paper award and the outstanding reviewer award of IEEE TRANSACTIONS ON POWER ELECTRONICS in 2014 and 2016, respectively, and the best paper award at IEEE PEDG 2016.



Zhe Chen (M'95-SM'98) received the B.Eng. and M.Sc. degrees from Northeast China Institute of Electric Power Engineering, Jilin City, China, and the Ph.D. degree from University of Durham, U.K.

Dr Chen is a full Professor with the Department of Energy Technology, Aalborg University, Denmark. He is the leader of Wind Power System Research program at the Department of Energy Technology, Aalborg University and the Danish Principle Investigator for Wind Energy of Sino-Danish Centre for Education and Research. His research areas are power systems, power electronics and electric machines, and his main current research interests are wind energy and modern power systems. He has led many research projects and has more than 360 publications in his technical field.



Frede Blaabjerg (S'86-M'88-SM'97-F'03) was with ABB-Scandia, Randers, Denmark, from 1987 to 1988. From 1988 to 1992, he was a Ph.D. Student with Aalborg University, Aalborg, Denmark. He became an Assistant Professor in 1992, Associate Professor in 1996, and Full Professor of power electronics and drives in 1998. His current research interests include power electronics and its applications such as in wind turbines, PV systems, reliability, harmonics and adjustable speed drives. He has received 17 IEEE Prize Paper Awards, the IEEE PELS Distinguished Service Award in 2009, the EPE-PEMC Council Award in 2010, the IEEE William E. Newell Power Electronics Award 2014 and the Villum Kann Rasmussen Research Award 2014. He was an Editor-in-Chief of the IEEE

TRANSACTIONS ON POWER ELECTRONICS from 2006 to 2012. He is nominated in 2014 and 2015 by Thomson Reuters to be between the most 250 cited researchers in Engineering in the world.